High interannual surface pCO$_2$ variability in the Southern Canadian Arctic Archipelago's Kitikmeot Sea.

Richard P. Sims[1,a], Mohamed Ahmed[1,2], Brian J. Butterworth[3,4], Patrick J. Duke[5], Stephen F. Gonski[6], Samantha F. Jones[1], Kristina A. Brown[7], Christopher J. Mundy[8], William J. Williams[7], Brent. G. T. Else[1],

[1]Department of Geography, University of Calgary, Calgary, Alberta, T2N 1N4, Canada
[2]Geology Department, Beni-Suef University, 101 Salah Salem St., Bani Sweif, 62511, Egypt
[3]Cooperative Institute for Research in Environmental Sciences, University of Colorado, Boulder, Colorado, USA
[4]NOAA Physical Sciences Laboratory, Boulder, Colorado, USA
[5]School of Earth and Ocean Sciences, University of Victoria, Victoria, British Columbia, Canada
[6]School of Marine Science and Policy, University of Delaware, Lewes, Delaware, USA
[7]Fisheries and Oceans Canada, Sidney, British Columbia, Canada
[8]Centre for Earth Observation Science, University of Manitoba, Winnipeg, MB R3T 2N2, Canada
[a]now at: Centre for Geography and Environmental Science, College of Life and Environmental Sciences, University of Exeter, Penryn campus, United Kingdom

Correspondence to: Richard P. Sims (richardpeter.sims@ucalgary.ac.uk)

Abstract. Warming of the Arctic due to climate change means the Arctic Ocean is now ice-free for longer as sea ice melts earlier and refreezes later. It remains unclear how the extended ice-free period will impact carbon dioxide (CO$_2$) fluxes due to scarcity of surface ocean CO$_2$ measurements. Baseline measurements are urgently needed to understand how air−sea CO$_2$ fluxes will spatially and temporally vary in a changing Arctic Ocean. It is uncertain whether the previous basin-wide surveys are representative of the many smaller bays and inlets that make up the Canadian Arctic Archipelago. By using a research vessel that is based in the remote Inuit community of Cambridge Bay (Ikaluqtuutiak, Nunavut), we have been able to reliably survey pCO$_2$ shortly after ice melt and access previously unsampled bays and inlets in the nearby region. We present four years of consecutive summertime pCO$_2$ measurements collected in the Kitikmeot Sea in the southern Canadian Arctic Archipelago. Overall, we found that this region is a sink for atmospheric CO$_2$ in August (average of all calculated fluxes over the four cruises was -8.3 mmol m^{-2} d^{-1}) but the magnitude of this sink varies substantially between years and locations (average calculated fluxes of 0.41, -7.70, -21.26 and -2.08 mmol m^{-2} d^{-1} during the 2016.2017,2018 and 2019 cruises respectively). Surface ocean pCO$_2$ varied by up to 142 µatm between years; this highlights the importance of repeat observations in the Arctic as this high interannual variability would not have been captured by sparse and infrequent measurements. We find that the pCO$_2$ value of the surface ocean at the time of ice melt is extremely important in constraining the magnitude of the air−sea flux throughout the ice-free season. Further constraining the flux in the Kitikmeot Sea will require a better understanding of how pCO$_2$ changes outside of the summer season. Surface ocean pCO$_2$ measurements made in the bays and inlets in the Kitikmeot Sea were ~20-40 µatm lower than in the main channels, and pCO2 measurements made close to ice breakup (i.e. within 2 weeks) were 50-100 µatm lower than measurements made >4 weeks after breakup. As basin-wide surveys of the CAA have focused on the deeper shipping channels and rarely measure

close to the ice break-up date, we hypothesize that there may be an observational bias in previous studies, leading to an underestimate of the CO_2 sink in the Canadian Arctic Archipelago. These high-resolution measurements constitute an important new baseline for gaining a better understanding of the role this region plays in the uptake of atmospheric CO_2.

1 Introduction

The Arctic Ocean plays an important role in the global carbon cycle as a sink for atmospheric carbon dioxide (CO_2). The solubility of CO_2 increases at low temperatures meaning that gas exchange and carbon drawdown is enhanced in cold polar surface waters; this is commonly known as the ocean solubility pump (Parmentier et al., 2013). Despite its role as a sink for CO_2, the magnitude of CO_2 uptake by the Arctic Ocean is poorly constrained as the region remains spatially and temporally under-sampled due to difficult seasonal access heavily skewing measurements to the ice-free summer period (DeGrandpre et al., 2020). Additionally, logistical constraints in poorly charted nearshore waters also tend to bias underway CO_2 measurements to established shipping routes and the deep ocean basins, leaving much of the Arctic coastal zone under-sampled in the Surface ocean CO_2 Atlas (SOCAT v2022) (Bakker et al., 2016). This is not a trivial oversight, given that the Arctic Ocean is encircled by coasts and their associated shelf seas: 53% of the $\sim 10.7 \times 10^6$ km^2 Arctic Ocean surface area is <200m in depth (Bates and Mathis, 2009).

The Arctic is already being heavily impacted by climate change (Landrum and Holland, 2020), with potentially devastating impacts on the Inuit and other indigenous communities who live there (Ford et al., 2008). It is not certain how the Arctic carbon system will respond to the present changes and how the effects of processes like ocean acidification will manifest and impact Inuit communities. Projecting long-term change in regions with complex biogeochemistry (i.e. the coastal domain) is particularly difficult. To better predict how the Arctic carbon system will change in the future requires baseline measurements, including detailed surveys and regular monitoring of oceanic pCO$_2$ that reflect the diverse nature of Arctic marine environments.

The Canadian Arctic Archipelago (CAA) is made up of numerous islands that cover 13% of the Arctic Ocean (Macdonald et al., 2010). The numerous islands account for the Canadian Arctic having 162,000 km of coastline (Wynja et al., 2015). The islands of the CAA form a complex bathymetry which is important in determining the circulation in the CAA (Wang et al., 2012). The majority of existing pCO$_2$ measurements made in the CAA were collected along the southern route through the Northwest Passage on the research icebreaker *CGGS Amundsen* (Ahmed et al., 2019). This large pCO$_2$ dataset was used to estimate a -7.7 ± 4 Tg C yr^{-1} sink for the CAA during the open water season (Ahmed and Else, 2019). The *CCGS Amundsen* pCO$_2$ dataset provides excellent broad spatial coverage of the CAA but the vast area surveyed was limited in temporal coverage and fine spatial detail. The *CCGS Amundsen* typically only transited through the central straits, channels, gulfs and

seas that make up the southern route through the Northwest Passage once each summer. The numerous bays and inlets that are off the main channel were not sampled, meaning that local-scale $p\text{CO}_2$ variability was potentially unaccounted for during

70   the synoptic scale sampling. This small-scale $p\text{CO}_2$ variability is difficult to predict empirically and may be better observed via regional studies. For example, the model of Ahmed et al. (2019) is known to underestimate $p\text{CO}_2$ by an average of ~26 µatm in Coronation Gulf and Dease Strait regions of the Kitikmeot Sea, likely due to river inflow. Understanding what caused this deviation from the model warrants further investigation and makes the Kitikmeot Sea a prime location for focused study.

75

Our understanding of the inorganic carbon system in the Kitikmeot Sea region comes from three distinct sources of measurements. Firstly, the 2010-2016 summertime ship measurements of $p\text{CO}_2$ in the central channel of the Kitikmeot presented by Ahmed et al. (2019). Their measurements show the region to be slightly undersaturated at the beginning of August, becoming slightly oversaturated in the middle of August through to the middle of September and then becoming

80   undersaturated again in early October. Coronation Gulf is one of the few areas of the CAA that was consistently observed to be supersaturated with CO_2 in summer. Oversaturation of $p\text{CO}_2$ in Coronation Gulf is likely a result of high summer surface seawater temperatures (CO_2 thermodynamics mean that a 1°C temperature increases $p\text{CO}_2$ by 4.23% (Takahashi et al., 1993)) and high river discharge, particularly to the west (Geilfus et al., 2018). The second source of carbonate system measurements in the region are CO_2 flux observations at the Qikirtaarjuk Island observatory in the Finlayson Islands in

85   Dease Strait (Butterworth and Else, 2018). Their measurements from the 2017 ice breakup season through to the summer indicate that there is CO_2 drawdown, and thus, undersaturation at breakup and for the first two weeks of open water. Near the end of July, the region transitions into a CO_2 source through to the end of August (Butterworth and Else, 2018). The region reverts to a sink in late August as the sea cools and surface $p\text{CO}_2$ declines; the region remains a sink until almost full ice cover in November (Butterworth et al., 2022). A similar pattern was observed in the summer of 2018, except notably, when

90   $p\text{CO}_2$ began to fall in late August the region did not revert all the way back into a sink (Butterworth et al., 2022). The third source of carbonate system measurements are provided by Duke et al. (2021) who report autonomous $p\text{CO}_2$ measurements at a depth of 7 m from an instrument installed on the Ocean Networks Canada (ONC) underwater sensor mooring in Cambridge Bay between August 2015 and August 2018. The sensor measurements from Cambridge Bay indicate that $p\text{CO}_2$ is oversaturated in winter and undersaturated by the start of June at the onset of sea ice melt (Duke et al., 2021). Their

95   measurements show that there is a short period of oversaturation in the middle of August coinciding with increased sea temperature, the ocean then quickly returns to a sink and remains undersaturated up until freeze-up (Duke et al., 2021).

All three sources of measurements indicate that there is notable interannual variability in surface $p\text{CO}_2$ in the Kitikmeot Sea. The ship-based measurements provide a snapshot of spatial variability across the wider region during the open-water season

100   whereas the time series from Qikirtaarjuk Island observatory and the ONC mooring provide insights into seasonal and interannual variability at specific locations. There are obvious shortcomings to both approaches. Icebreaker-based studies

may under-represent small-scale variability that exists in nearshore regions that are inaccessible due to the vessel's large draft. Whereas the fixed observatories may over-represent temporal variability which is location-specific; for example, the ONC mooring is in an enclosed Bay close to the outlet of a large river (Manning et al., 2020) and the flux footprint of the

105 Qikirtaarjuk Island observatory spans a hotspot for mixing and productivity (Dalman et al., 2019). Given the limitations of each of these data sources, there is a need to understand how representative these data sources are of the wider Kitikmeot Sea region.

In this paper, we present surface pCO$_2$ measurements made during annual summertime surveys of the Kitikmeot Sea

110 between 2016 and 2019. We use these new pCO$_2$ measurements to determine the magnitude of CO$_2$ uptake in the Kitikmeot Sea shortly after ice breakup. These new pCO$_2$ measurements also allow us to bridge the gap between previous measurements which were made at contrasting spatial scales (e.g. the low spatial variability point-scale observation from the local carbon observatories and the large-scale CAA-wide pCO$_2$ measurements). We use our new measurements to explore whether there are small-scale regional pCO$_2$ differences in the inlets and bays of the CAA which are not adequately

115 represented by CAA-wide sampling. We also use our new measurements to explore pCO$_2$ variability in the proximity of these observatories to see whether they are representative of the wider region. In attempting to unify existing measurements we aim to unravel the seasonal and interannual variability of pCO$_2$ in the region.

2 Methods

2.1 Oceanographic setting

120 The Kitikmeot Sea (Figure 1) is a shallow shelf sea within the CAA that encompasses Coronation Gulf to the west, linked via Dease Strait to Queen Maud Gulf in the East, Bathurst Inlet to the South, and Chantrey Inlet to the Southeast (Williams et al., 2018). The communities of Cambridge Bay, Kugluktuk, and Gjoa Haven, Nunavut, are the main year-round settlements in the Kitikmeot Sea region. River inputs from mainland Canada and snow and ice melt provide a considerable source of freshwater in the region (Williams et al., 2018), resulting in some of the lowest salinity surface waters in the CAA

125 (Ahmed et al., 2019). The Kitikmeot sea is nutrient-limited (Back et al., 2021), and as a result chlorophyll concentrations are also low in the region (Kim et al., 2020). Modelling results suggest that the stratification regime in Dease Strait and Queen Maud Gulf is characterised by a ~40 m warm fresh surface layer and a cold salty bottom layer which extends down to around 100 m (Xu et al., 2021). Coronation Gulf has a three layer regime composed of a 40 m warm fresh surface layer, a colder salty layer down to 100 m and a stable deep layer down to 350 m (Xu et al., 2021). Vertical mixing in the Kitikmeot Sea is

130 prohibited by strong stratification throughout most of the year; however after sea ice breakup wind driven mixing gradually deepens the surface mixed layer resulting in an almost fully mixed water column in Dease Strait (Xu et al., 2021).

The oceanographic boundary for the Kitikmeot Sea has been designated as where the shelf shoals to <30 m in the west (Dolphin and Union Strait) and northeast (Victoria Strait) (Williams et al., 2018). At the Dolphin and Union Strait, warm

135 fresher surface seawater flows out across the sills while subsurface flows of more saline nutrient-rich Pacific waters enter the sea. Another feature of the Kitikmeot Sea is that strong tidal currents in narrow channels can keep certain areas ice-free in winter (Williams et al., 2018). Strong tidal currents beneath sea ice such as around the Finlayson Islands in Dease Strait act to slow winter sea ice growth and enhance primary production by introducing nutrients (Dalman et al., 2019). First-year sea ice dominates the Kitikmeot Sea although some multiyear ice may be blown into Queen Maud Gulf from the northern part of

140 the CAA (Xu et al., 2021). Seawater temperatures across the Kitikmeot Sea vary considerably throughout the year; they are around -2°C in winter and reach upwards of 10°C in summer (Xu et al., 2021). The bounding sills, large freshwater inputs and low nutrient loads make the Kitikmeot Sea unique within the CAA.
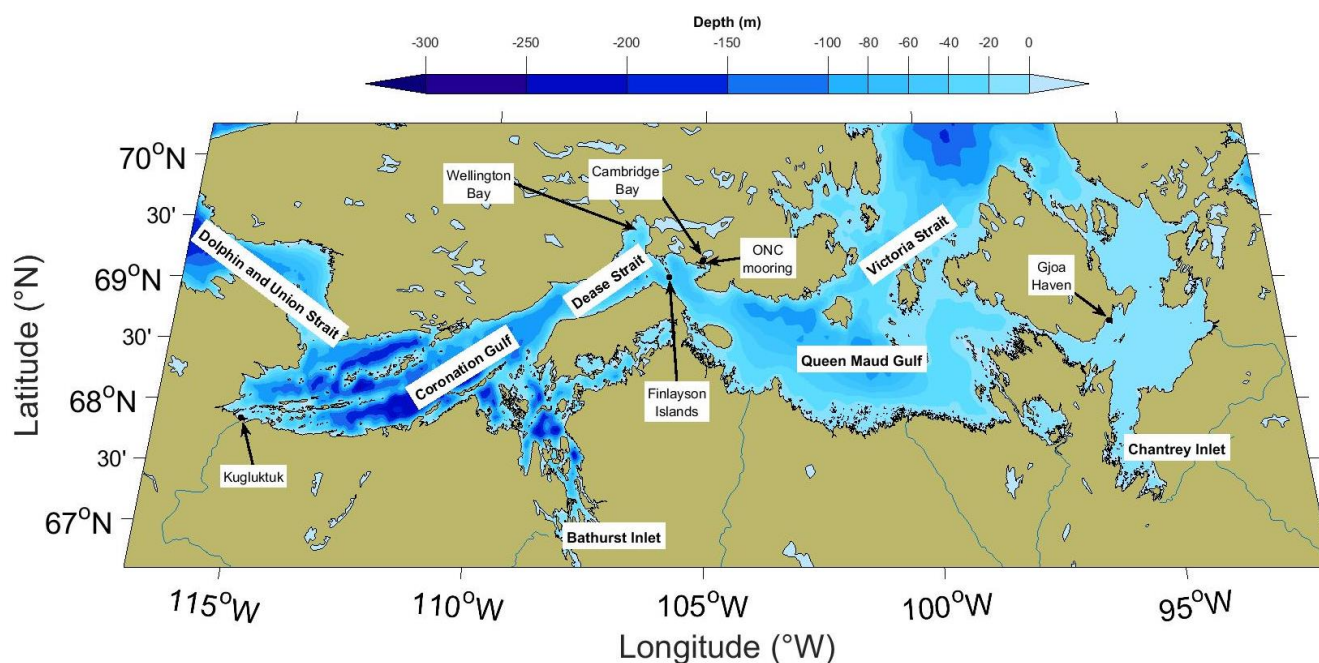
Figure 1: A map of the Kitikmeot Sea. The main settlements in the region (Cambridge Bay, Kugluktuk and Gjoa Haven) are labelled as are the Ocean Networks Canada mooring and the Qikirtaarjuk Island observatory where the eddy covariance tower is located. Shoreline data is from the World Vector Shoreline database and river data is taken from the CIA World Data Bank II (WDBII), both of which were accessed via the Global Self-consistent, Hierarchical, High-resolution Geography Database (GSHHG) (Wessel and Smith, 1996). Bathymetry data is taken from the 2-minute Gridded Global Relief Data (ETOPO2) v2 database (NGDC, 2006). This map was made using tools from the M_Map Matlab plotting package (Pawlowicz, 2020).

2.2 Field campaign description

145 Annual oceanographic surveys of the summertime surface seawater partial pressure of carbon dioxide (pCO$_2$ $_{(sw)}$) were conducted between 2016 and 2019 in the Kitikmeot Sea (Figure 1) aboard the *RV Martin Bergmann* as part of the Marine

Environmental Observation, Prediction and Response Network (MEOPAR) and Kitikmeot Sea Science Study (K3S)
programs (cruise details in table S1). In each of the four years, an underway pCO$_2$ system was deployed on cruises
conducted under ice-free conditions between early August and mid-September. The Canadian High Arctic Research Station

150   in Cambridge Bay, Nunavut acted as a staging ground for this work since Cambridge Bay is the home port for the *RV Martin
Bergmann*.

Between 2016 and 2019, the cruise track varied from year to year depending on the focus of the work (Figure 2). The first
week of each summer field season was typically used to complete work for the MEOPAR program, the majority of the ship
time was spent in the proximity of Cambridge Bay, the Finlayson Islands, Wellington Bay and the western region of Queen

155   Maud Gulf. Cruises in mid to late August were used to conduct work for the K3S program; the ship typically ventured
further afield heading into Bathurst Inlet, the central region of Queen Maud Gulf and Chantry Inlet. The opportunistic nature
of the data collection meant that data density varied between regions, as not every region was surveyed each year.

Sea ice concentrations in the months preceding each annual survey are taken from the daily gridded 3.125 km AMSR2
satellite radiometer product (Spreen et al., 2008). To determine weeks since open water, the nearest point on the AMSR2

160   grid was determined for each pCO$_{2\ (sw)}$ measurement. The time between the measurement and when sea ice concentration fell
constantly below the threshold value for the marginal ice zone (85%) (Cruz-García et al., 2021) was then calculated.
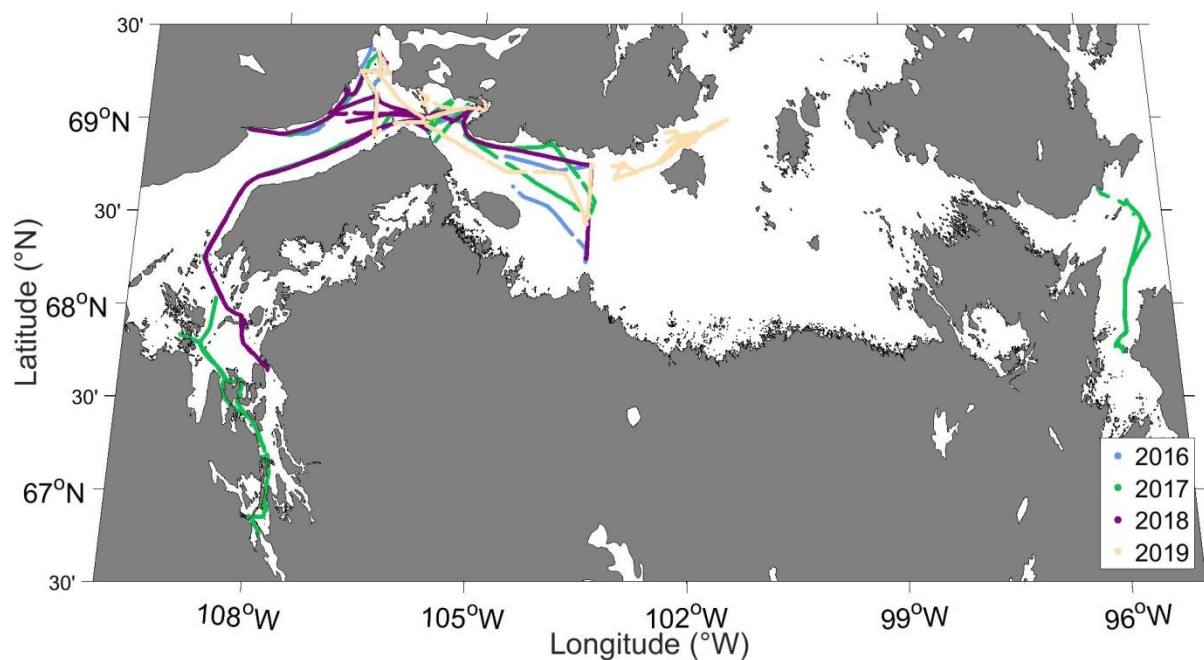
Figure 2: Ship cruise tracks for each of the four surveyed years.

2.3 Underway system

The *RV Martin Bergmann* is a 20 m repurposed commercial fishing trawler from Newfoundland with a draft of 3.4 m (Figure 3a and 3b). The ship does not have its own dedicated integrated underway system; instead surface seawater was sampled from an inlet at a depth of ~1 m through ~2 m of 1/2" ID PVC tubing securely draped over the bulwark of the vessel through an external hatch (Figure 3c and 3d). A Waterra Tempest WSP-12V-3 submersible pump was used to pump surface seawater through this inlet tubing at a rate of 10 L min^{-1}. *In situ* surface seawater temperature (SST $_{(1m)}$) was measured by a Campbell Scientific 107 temperature sensor attached to the tubing inlet.

Upon entering the ship, the flow of seawater passed through a SoMAS MSRC VDB-1 vortex debubbler and was then split between several instruments via Tygon tubing (Figure 3). The Idronaut Ocean Seven 315 On-line module thermosalinograph measured seawater temperature (SST $_{(tsg)}$) and salinity at a seawater flowrate of 0.5 L min^{-1}. The Wetlabs ECO BBFL2B Triplet measured fluorescence at a flowrate of 2.5 L min^{-1}. The ECO fluorescence sensor output was post-processed to remove spikes from bubbles and particles but was not calibrated against *in situ* measurements. A flow of 2 L min^{-1} was directed to the seawater equilibrator. Instrument flowrates were set with manual flowmeters so that the internal instrument volumes and associated tubing of the Idronaut, ECO and equilibrator were flushed at the same rate, this meant that approximately half of the 10 L min^{-1} flow from the pump was not analysed and was discarded overboard.

Figure 3: (a) Image of the *RV Martin Bergmann* at sea taken in August 2017, (b) image of *RV Martin Bergmann* stored on its trailer taken on a mild day in May 2019, (c) labelled photograph of the underway system installed in the ship's lab space, and (d) detailed cross sectional schematic of the underway system with labelled instruments and flowrates. Instruments mounted to the wall are shown with a yellow background, water circulation is shown in blue and air circulation is shown in red.

A made to order Sunburst Sensors underway SuperCO$_2$ system measured surface seawater CO$_2$; this system was previously

180   described by Evans et al. (2019), and follows the general recommendations of Dickson et al. (2007) SOP5. A Permapure liqui-cel 2.5X8 series membrane contactor served as the equilibrator for the pCO$_2$ system, the waterside seawater flowrate

for the equilibrator was approximately 2 L min^{-1}. Seawater temperature was measured at the equilibrator seawater inlet using a thermistor ($T_{(equ)}$). The gas counter flow into the equilibrator was supplied by an air pump at a flowrate of 100 ml min^{-1}. CO_2 has been shown to fully equilibrate in this model liqui-cel when set up in a single pass setup at these water and gas

185 flowrates (Sims et al., 2017). The system does not utilise a dryer and thus requires a water vapour correction in post-processing. For additional accuracy, the inbuilt H_2O sensor was calibrated with a LI-610 Portable Dew Point Generator on-site before each deployment. The SuperCO$_2$ system has a standard multi-position valve and alternates between equilibrator air, atmospheric samples, and three gas standards. The timing of the valve switching was set so that each of the three CO_2 standards (mixing ratios (xCO_2) of 255.1, 409.9, and 566.4) were flushed through the system at 200 ml min^{-1} for 5 minutes

190 every 6 hours. Standard gases were certified at the University of Manitoba against standards obtained from Environment and Climate Change Canada, and are thus traceable to World Meteorological Organization standards. The SuperCO$_2$ system has an integrated air pump configured to make atmospheric measurements; these measurements were not used due to contamination from the ship's exhaust. The SuperCO$_2$ system also measures atmospheric pressure $P_{(atm)}$.

195 Variables were logged every minute: xCO_2 and related variables were logged to the computer of the SuperCO$_2$ system, the data recorded by the ECO were logged to a separate data file, and the latitude and longitude recorded with a Garmin GPS16X-HVS GPS unit were logged to a Campbell Scientific CR300 data logger. The CO_2 measured by the system was processed following (Dickson et al., 2007) SOP 5. Partial pressure of CO_2 (pCO_2) is measured by the Licor 850 in the SuperCO$_2$ system, this is converted to the gas mixing ratio of CO_2 (xCO_2) using the pressure in the Licor (P_{licor}). The xCO_2 is

200 calibrated using a piecewise linear interpolation in time with the three standards. The partial pressure is then determined in the equilibrator ($pCO_{2\ (equ)}$) using the $P_{(atm)}$ and assuming full humidity. $pCO_{2\ (equ)}$ is converted to $pCO_{2\ (1m)}$ using the $T_{(equ)}$, $SST_{(1m)}$, and the fractional temperature change constant of (Takahashi et al., 1993). The depth of the seawater inlet was validated each year by comparing the thermosalinograph salinity and the in situ temperature sensor with surface temperature and salinity from CTD rosette measurements at the surface. There was no in situ temperature sensor during the 2017 and

205 2018 field seasons, the warming was then characterised from T(equ) and CTD rosette measurements following Ahmed et al. (2019), details of this can be found in the supplementary materials. Additionally, median observational values of -0.17°C and +0.1 were added to the in situ temperature and salinity to account for ubiquitous skin effects when calculating interfacial seawater pCO_2 (Woolf et al., 2019).

210 Using an identical setup DeGrandpre et al. (2020) estimate the pCO_2 uncertainty as ± 5 μatm, this is the uncertainty for our 2016 and 2019 measurements. In 2017 and 2018, there is an additional uncertainty component associated with using an empirical relationship to obtain $SST_{(1m)}$. This additional uncertainty is calculated by taking the RMSD values from those empirical relationships (2017 = 0.49°C, 2018 = 0.64°C) and propagating them through the temperature equation for $pCO_{2\ (1m)}$ (Takahashi et al., 1993). This results in an additional 2.09% and 2.74% uncertainty in $pCO_{2\ (1m)}$, these values are similar to

215 the 2% uncertainty reported by (Ahmed et al., 2019) following the same method. For a $pCO_{2\ (equ)}$ value of 300 μatm this

equates to an additional 6.3 and 8.2 µatm uncertainty for each year respectively. Propagating uncertainties gives final uncertainties of 8.04 and 9.60 µatm for 2017 and 2018 respectively, these calculation of these uncertainties is consistent with the International Bureau of Weights and Measures (BIPM) Guide to the expression of uncertainty in measurement (GUM) methodology (JCGM, 2008).

220

The standard system configuration during the four cruises is detailed above; changes from this configuration during specific cruises are detailed in the supplementary materials (Table S2). There are several logistical aspects associated with deploying, operating, and maintaining an underway $p\text{CO}_2$ system in a remote Arctic location on a small vessel like the *RV Martin Bergmann;* this is discussed further in supplementary materials.

225 **2.4 Calculations: Air sea CO2 fluxes**

In the absence of a reliable ship-based atmospheric CO_2 record, hourly measurements are taken from the atmospheric observatory in Barrow Alaska (71.32°N,156.61°W) (K.W. Thoning, 2020;Peterson et al., 1987). Despite the long distance between Barrow and the Kitikmeot Sea (around 1800 km), atmospheric CO_2 should be quite similar at both locations as the atmosphere is well mixed for a long residence time gas like CO_2 and both locations are remote northern sites away from

230 biogenic and industrial emissions. Wind speed adjusted to a reference height of 10 m (U_{10}) is taken from the Qikirtaarjuk Island observatory (Butterworth and Else, 2018) for the 2017 and 2018 field seasons whereas a four times daily record of U_{10} from the NCEP-DOE v2 reanalysis product (Kalnay et al., 1996) is used for 2016 and 2019 field seasons.

The air-sea fluxes of CO_2 (F, mmol m^{-2} d^{-1}) is calculated as

$$F_{(sea-air)} = k_W\, k_0\, \Delta p\text{CO}_2\, SF$$

235 The water phase gas transfer velocity (k_w, cm hr^{-1}) is calculated using U_{10} and the parameterisation of Nightingale et al. (2000), a unitless Schmidt number (Sc) normalised to a Sc of 660 (Wanninkhof, 2014) is used to scale k_w.

$$k_W = (0.222\,(U_{10})^2 + 0.333\,(U_{10}))\,(Sc/660)^{-1/2}$$

$\Delta p\text{CO}_2$ (µatm) is the partial pressure difference between the seawater interface and air $\Delta p\text{CO}_2 = p\text{CO}2_{(sw)} - p\text{CO}2_{(air)}$. The solubility of CO_2 in seawater ($k_{0,}$ mol L^{-1} atm^{-1}) is taken from (Weiss, 1974). A unit scaling factor (SF) of 0.24 is used to

240 convert the units of k_w to md^{-1}. The Schmidt number and solubility are calculated using the *in situ* temperature and salinity values adjusted for skin effects (Woolf et al., 2019).

Direct measurements of the air–sea CO_2 fluxes (F $_{(sea-air)}$) made using the micrometeorological eddy covariance technique (Butterworth and Else, 2018) can be used to infer $p\text{CO}2_{(sw)}$ by rearranging the flux equation as follows using $p\text{CO}2_{(air)}$ from the Licor 7200 at the Qikirtaarjuk Island observatory and SST and SSS from a mooring at 13m which was 1 km from the

245 tower (Butterworth et al., 2022).

$$(F_{(sea-air)} / k_W\, k_0\, SF) + p\text{CO}2_{(air)} = p\text{CO}2_{(sw)}$$

3. Results

To facilitate comparisons between cruises made in different years, observations have been partitioned into separate
250 oceanographic zones based on the local geography, observational data density, previous $p\text{CO}_2$ $_{(sw)}$ measurements, and
proximity to the local carbon observatories (Figure 4a). Bathurst Inlet and Chantry Inlet were designated zones based on
their large freshwater inputs. The Finlayson Islands and Cambridge Bay are where the Qikirtaarjuk Island observatory and
ONC mooring are located, respectively; these regions were also heavily surveyed because the *RV Martin Bergmann* often
returned to port in Cambridge Bay and passed the islands to access Wellington Bay and Bathurst Inlet. Wellington Bay
255 (Figure 1) is a shallow, partially enclosed basin for which a relatively large amount of data was collected due to annual fish-
tagging surveys associated with the local subsistence char fishery (Harris et al., 2020). All the measurements in the Dease
Strait West zone were made in the central channel and are in the same approximate geographically region to those collected
by Ahmed et al. (2019). Most of the measurements in the Queen Maud Gulf zone were made in the west; the box is large
enough to include sparse measurements in the central and Northern regions which do not warrant being considered
260 separately.

Observations of temperature, salinity, $p\text{CO}_{2(sw)}$, fluorescence, U_{10}, and CO_2 flux during the four field seasons are plotted as
time series and coloured by the sub-region of the measurement (Figure 4b-4g). Summary statistics (mean, standard
deviation, and range) of each variable in each region for all four cruises are presented in Table 1. Plots showing the timing of
265 the cruise track, temperature, salinity, $p\text{CO}_{2(sw)}$, and chlorophyll-a fluorescence can be found in the supplementary materials
(Figures S2 to S6).
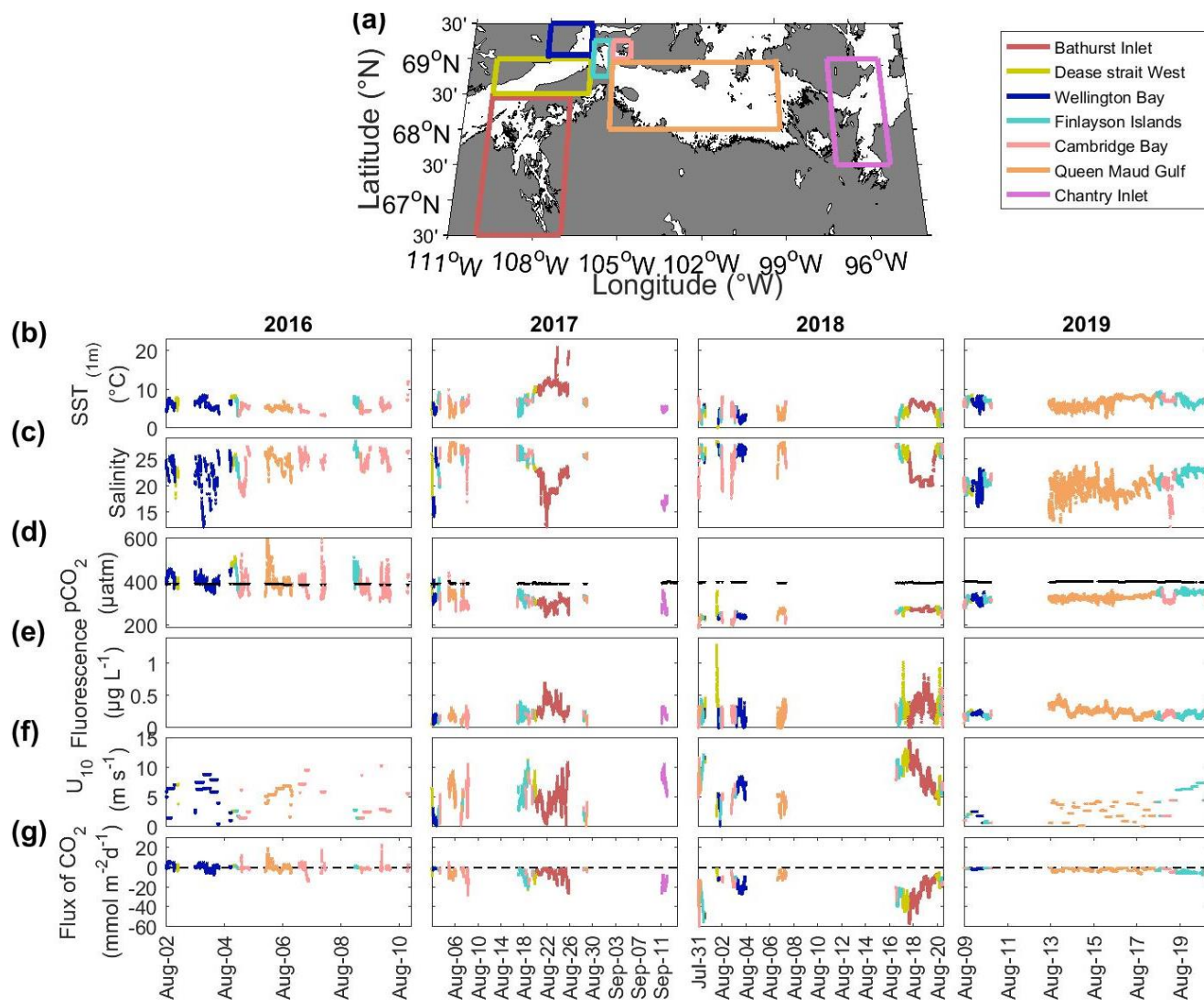
Figure 4: (a) Map of Kitikmeot Sea showing the region surveyed by the *RV Martin Bergmann* between 2016 and 2019. The sampled region was subdivided as described in the main text; these sub regions are shown as coloured boxes and correspond to the names in the legend. Timeseries subplots of underway surface ocean (1m) observations for 2016 through to 2019 of (b) SST (1m), (c) salinity, (d) pCO$_2$ (sw) (with pCO$_2$ (atm) in black), (e) fluorescence, (f) U10, and (g) flux of CO$_2$ (no flux is indicated by a dashed black line). The time series data are coloured according to the sampling regions in panel (a). The period of measurements was not consistent between years so the date label tick spacing and the range are different between years. Large data gaps correspond to when the ship was in port between cruise legs or data outages.

SST $_{(1m)}$ interannual variability was on the order of several degrees (Figure 4b), for example the SST $_{(1m)}$ in 2018 was cooler than SST $_{(1m)}$ in 2017 (Table 1). Inter-region SST $_{(1m)}$ differences of ~10°C were observed during all four surveys (Figure 4b). Summertime warming of several degrees can be observed in the data for certain sub regions which were visited multiple times such as Cambridge Bay in 2016 and Queen Maud Gulf in 2019 (Figure 4b). Some of the sub regions were considerably

270

warmer than others (e.g., Bathurst Inlet in 2017 and 2018), whereas other regions like Queen Maud Gulf were consistently colder (tabl1).

There was large interannual variability in surface salinity; for example salinity in 2019 was generally lower than 2018 (Figure 4c). Salinity values were much lower in Chantry Inlet in 2017 and Bathurst Inlet in both 2017 and 2018 relative to the salinities in other regions in those years (Table 1). Salinity ranges on the order of ~5 – 10 were observed between regions in all years. The salinity data are marked by rapid changes of ~5 which did not coincide with equivalent temperature changes (Figure 3c); these salinity transitions are evident in the 2017 and 2018 Bathurst Inlet data, much of the Cambridge Bay data and the Wellington Bay data from 2016 and 2019. There is evidence of freshening in the first week of August 2016 and in Queen Maud Gulf in 2019, but there does not appear to be a seasonal freshening trend in 2017 or 2018.

There was high interannual $p\mathrm{CO}_{2\,(sw)}$ variability (Table 1), where $p\mathrm{CO}_{2\,(sw)}$ was close to equilibrium with the atmosphere in 2016 and highly undersaturated in 2017, 2018 and 2019 (Figure 4d). The $p\mathrm{CO}_{2\,(sw)}$ interannual variability was larger than the observed regional variability each year(Table 1). $p\mathrm{CO}_{2\,(sw)}$ increased across all regions in both 2018 and 2019; this is also seen as increases on return visits to the Finlayson Islands and Cambridge Bay several weeks apart from each other (Figure 4d). In all four years, Cambridge Bay had low $p\mathrm{CO}_{2\,(sw)}$ relative to the other regions. Low $p\mathrm{CO}_{2\,(sw)}$ values were also seen in Bathurst Inlet, Chantry Inlet and Wellington Bay. Many low $p\mathrm{CO}_{2\,(sw)}$ regions were also low salinity regions. Fluorescence was generally low throughout all the cruises in all years except for the relatively higher fluorescence signal in Bathurst Inlet and around the Finlayson Islands (Figure 4e). The air–sea CO_2 flux (Figure 4g) reflects the trends in the predictor variables, particularly $p\mathrm{CO}_{2\,(sw)}$ and U_{10} (Figure 4d and 4f). The air–sea flux calculated in 2016 was small (0.41 mmol m^{-2} d^{-1} reflecting the fact that the $p\mathrm{CO}_{2\,(sw)}$ was close to equilibrium with the atmosphere. In 2017 and 2019 $p\mathrm{CO}_{2\,(sw)}$ was quite undersaturated (309 and 330 µatm respectively), the 2017 flux was larger (-7.7 mmol m^{-2} d^{-1}) than the 2019 flux (-2.1 mmol m^{-2} d^{-1}) as the wind speed was very low in 2019 (3.1 ms^{-1}).

Table 1: Underway surface ocean (1m) observation summary table for the *RV Martin Bergmann* cruises from 2016 through 2019. Geographical sub regions are defined in Figure 4a. Top line is the mean ± 1 standard deviation and the bottom row is the measurement range. Table averages are the average of all the observations for each variable for each year and have not been scaled to the spatial extent of each region. Whilst yearly averages are provided, as the spatial extent of the measurements from each year was different, comparisons between years should be made with caution.

Year	Sub region	No of obs	$SST_{(1m)}$ (°C)	Salinity	$pCO2_{(sw)}$ (µatm)	Fluorescence	U_{10} (m s^{-1})	Flux (mmol m^{-2} d^{-1})
2016	Dease Strait West	376	7.62 ± 0.75 4.71– 8.50	23.58 ± 1.54 17.74 – 26.08	444.95 ± 46.08 370.10 – 519.84	-	4.25 ± 2.31 1.12 – 7.22	0.77 ± 1.48 -2.93 – 3.10
	Wellington Bay	1523	6.35 ± 1.10 3.68 – 8.66	22.37 ± 3.11 12.21 – 26.84	411.52 ± 26.57 347.26 – 463.81	-	6.05 ± 2.23 0.58 – 8.91	0.81 ± 2.64 -7.27 – 6.38
	Finlayson Islands	412	6.30 ± 1.46 3.32 – 8.25	25.67 ± 1.77 21.01 – 28.57	428.09 ± 39.42 342.34 – 512.69	-	2.19 ± 0.59 1.55 – 2.92	0.58 ± 0.76 -0.67 – 2.30
	Cambridge Bay	2051	5.18 ± 1.38 3.18 – 12.13	24.42 ± 2.29 18.06 – 27.51	384.59 ± 40.72 311.52 – 598.99	-	4.22 ± 2.69 1.50 – 10.37	-0.18 ± 3.85 -13.93 – 23.58
	Queen Maud Gulf	1173	5.38 ± 0.56 4.22 – 7.14	24.61 ± 1.54 20.71 – 27.37	404.92 ± 53.00 337.11 – 687.37	-	5.93 ± 1.08 1.55 – 6.97	0.75 ± 3.76 -5.33 – 20.06
	Average all	5535	5.80 ± 1.34 3.18 – 12.13	23.93 ± 2.57 12.21 – 28.57	403.65 ± 44.44 311.52 – 687.37	-	4.94 ± 2.45 0.58 – 10.37	0.41 ± 3.32 -13.93 – 23.58
2017	Bathurst Inlet	7452	11.27 ± 1.96 8.56 – 21.14	20.78 ± 2.04 11.04 – 23.88	302.27 ± 18.57 242.22 – 350.96	0.32 ± 0.12 0.10 – 0.71	4.56 ± 2.23 0.38 – 10.91	-5.80 ± 4.97 -26.27 – -0.12
	Dease Strait West	1137	8.27 ± 1.93 3.40 – 10.60	23.21 ± 1.59 14.63 – 26.04	321.91 ± 10.71 301.44 – 381.48	0.18 ± 0.07 0.04 – 0.29	6.89 ± 2.32 0.30 – 11.43	-9.62 ± 5.32 -22.07 – -0.06
	Wellington Bay	847	5.04 ± 0.76 3.55 – 7.20	20.08 ± 4.60 14.23 – 27.22	327.07 ± 13.25 300.42 – 411.75	0.14 ± 0.03 0.07 – 0.22	1.27 ± 0.60 0.29 – 3.12	-0.55 ± 0.44 -2.34 – 0.09
	Finlayson Islands	3491	6.95 ± 0.83 3.08 – 9.39	25.18 ± 1.38 19.86 – 27.60	331.18 ± 14.07 284.14 – 418.75	0.20 ± 0.06 0.04 – 0.42	4.53 ± 2.31 0.43 – 11.12	-5.05 ± 4.21 -20.46 – -0.00
	Cambridge Bay	1951	6.47 ± 0.73	26.14 ± 1.48	313.20 ± 24.52	0.15 ± 0.06	5.05 ± 2.46	-7.20 ± 6.36

Year	Site	N						
			3.63 – 9.99	17.09 – 28.14	266.37 – 443.82	0.00 – 0.36	0.43 – 10.69	-27.52 – 6.16
	Queen Maud Gulf	1519	4.97 ± 1.23 2.78 – 7.50	27.25 ± 1.05 24.58 – 28.31	342.14 ± 10.05 314.16 – 376.45	0.17 ± 0.03 0.07 – 0.32	6.64 ± 2.28 0.29 – 9.46	-6.16 ± 2.95 -12.76 – -0.07
	Chantry Inlet	1247	4.99 ± 0.38 4.09 – 5.76	16.71 ± 0.61 15.45 – 18.25	291.56 ± 31.46 250.07 – 363.39	0.22 ± 0.06 0.07 – 0.34	8.11 ± 1.31 5.18 – 10.73	-16.55 ± 4.11 -26.23 – -7.18
	Average all	19730	8.00 ± 3.07 2.78 – 21.14	22.59 ± 3.44 11.04 – 28.31	308.55 ± 28.80 224.83 – 443.82	0.23 ± 0.11 0.00 – 0.71	5.19 ± 2.61 0.29 – 11.43	-7.70 ± 6.70 -29.73 – 6.16
2018	Bathurst Inlet	3215	5.85 ± 0.92 2.86 – 7.58	21.86 ± 1.91 19.81 – 27.52	274.34 ± 6.07 263.43 – 291.23	0.37 ± 0.15 -0.01 – 0.84	8.89 ± 2.27 4.79 – 14.69	-23.65 ± 10.81 -56.85 – -6.96
	Dease Strait West	1516	3.30 ± 1.82 -1.33 – 6.08	26.83 ± 1.01 24.42 – 28.50	272.02 ± 17.12 228.31 – 359.15	0.39 ± 0.25 0.06 – 1.30	8.38 ± 3.07 1.88 – 13.16	-22.94 ± 13.81 -52.05 – -1.61
	Wellington Bay	1414	3.04 ± 1.23 1.22 – 6.19	26.73 ± 0.80 24.48 – 27.93	244.40 ± 7.04 232.31 – 266.22	0.20 ± 0.11 -0.16 – 0.46	6.85 ± 2.12 0.28 – 11.90	-20.84 ± 9.17 -50.83 – -9.08
	Finlayson Islands	1352	3.24 ± 1.49 0.45 – 5.87	26.62 ± 1.02 24.68 – 28.07	259.49 ± 14.51 228.82 – 284.74	0.24 ± 0.11 -0.07 – 0.62	8.29 ± 2.36 1.41 – 12.32	-25.93 ± 10.26 -55.55 – -9.07
	Cambridge Bay	972	5.07 ± 1.90 1.33 – 8.22	23.80 ± 3.11 17.66 – 27.95	228.59 ± 20.23 193.07 – 271.62	0.21 ± 0.11 -0.27 – 0.62	6.23 ± 1.98 2.33 – 11.76	-17.94 ± 11.36 -59.63 – -3.19
	Queen Maud Gulf	1043	3.55 ± 0.90 1.87 – 5.77	27.06 ± 1.17 21.56 – 28.20	260.24 ± 14.14 227.45 – 282.02	0.18 ± 0.13 -0.19 – 0.45	4.70 ± 1.66 1.61 – 10.31	-9.17 ± 6.82 -39.80 – -1.25
	Average all	9512	4.32 ± 1.82 -1.33 – 8.22	24.82 ± 2.83 17.66 – 28.50	261.19 ± 19.70 193.07 – 359.15	0.29 ± 0.18 -0.27 – 1.30	7.70 ± 2.71 0.28 – 14.69	-21.26 ± 11.80 -59.63 – -1.25
2019	Wellington Bay	718	6.78 ± 0.97 3.82 – 8.56	19.81 ± 1.79 16.08 – 23.35	316.29 ± 13.72 289.15 – 354.95	0.22 ± 0.02 0.17 – 0.28	1.92 ± 0.70 0.64 – 2.64	-1.15 ± 0.49 -1.87 – -0.12
	Finlayson Islands	2870	7.37 ± 0.96 4.74 – 9.65	21.72 ± 1.24 18.13 – 24.21	346.16 ± 15.22 285.01 – 376.12	0.20 ± 0.04 0.11 – 0.31	4.82 ± 2.35 0.64 – 7.47	-3.07 ± 1.95 -7.11 – -0.16
	Cambridge Bay	1097	7.20 ± 0.55 5.21 – 8.81	20.03 ± 2.05 12.23 – 22.61	316.70 ± 14.44 278.34 – 366.70	0.21 ± 0.04 0.08 – 0.32	2.63 ± 1.46 0.71 – 4.50	-2.09 ± 1.74 -5.30 – -0.25

Queen Maud Gulf	6192	6.72 ± 1.29 2.86 – 8.81	19.47 ± 1.79 13.07 – 24.54	327.94 ± 8.02 291.33 – 362.30	0.26 ± 0.07 0.11 – 0.52	2.60 ± 1.44 0.10 – 5.87	-1.79 ± 1.40 -6.20 – -0.02
Average all	11058	6.96 ± 1.16 2.86 – 9.65	20.12 ± 1.93 12.23 – 24.54	330.71 ± 15.15 278.34 – 376.12	0.24 ± 0.07 0.08 – 0.52	3.13 ± 1.96 0.10 – 7.47	-2.08 ± 1.65 -7.11 – -0.02

4. Discussion

Presented in the results above are the multiyear summertime $p\text{CO}_{2\,(sw)}$ observations made on *RV Martin Bergmann*. These data reveal the spatial and inter-annual variability of $p\text{CO}_{2\,(sw)}$ near the beginning of the open-water season in the Kitikmeot Sea. To maximise the value of the $p\text{CO}_{2\,(sw)}$ observations made on *RV Martin Bergmann* we will now present and discuss these new measurements alongside previous measurements and in the context of our current understanding of the carbonate system in the region.

4.1 Local scale – comparisons with the ocean carbon observatories

The two local observatories, the ONC mooring in Cambridge Bay and the Qikirtaarjuk Island observatory, provide measurements throughout the year that are not readily possible with shipboard observations. $p\text{CO}_{2\,(sw)}$ is directly measured on the ONC mooring whereas $p\text{CO}_{2\,(sw)}$ is calculated from the flux derived using measurements from the Qikirtaarjuk Island observatory eddy covariance "EC tower". By taking the $p\text{CO}_{2\,(sw)}$ observations from these two observatories alongside the new *RV Martin Bergmann* measurements we can create a multiyear timeline of $p\text{CO}_{2\,(sw)}$ in the region (Figure 5). It should be noted that the three measurement sources in Figure 5 are not co-located, the Qikirtaarjuk Island observatory on the Finlayson Islands is 35 km west of the ONC mooring (Figure 1) and the Bergmann measurements span a slightly wider area (Figure 2). Despite the spatial disparity in these measurements, it should also be acknowledged that for calculations of global

310   CO_2 flux on a 1° x 1° grid, the majority of these measurements would fall within the same grid cell. It might be expected that

on these sorts of spatial scales the measurements should agree close to perfectly, but that is not the case (Figure 5).
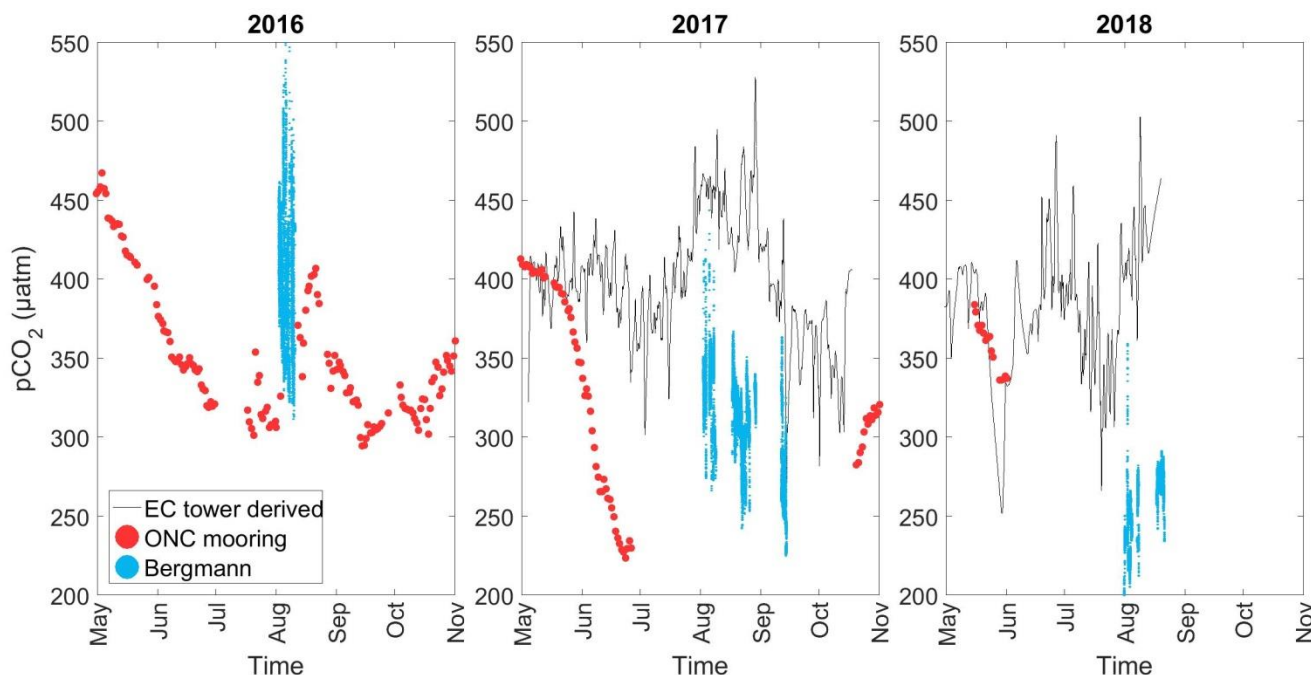
Figure 5: Surface $pCO_{2\ (sw)}$ from across the Kitikmeot Sea made in (a) 2016, (b) 2017 and (c) 2018. $pCO_{2\ (sw)}$ measurements from the ONC mooring are shown as red dots, all $pCO_{2\ (sw)}$ measurements from the *RV Martin Bergmann* are shown as blue dots and $pCO_{2\ (sw)}$ inferred from Eddy covariance at the Qikirtaarjuk Island observatory are shown as a black line.

The *RV Martin Bergmann* $pCO_{2\ (sw)}$ data are much lower in 2017 (Figure 5b) and 2018 (Figure 5c) relative to the values

predicted from the EC tower, even when measurements were made in the footprint of the EC tower (18:30 – 23:10 3rd

315   August 2017 $pCO_{2\ (sw)}$ from the tower was 414.67 and from *RV Martin Bergmann* was 344.21, 05:50– 06:40 August 1st

2018 $pCO_{2\ (sw)}$ from the tower was 408.69 and from *RV Martin Bergmann* was 237.40). The large differences between the

methods can not be reasonably explained by changes due to SST as this would require an extremely large temperature

gradient ~5–10 °C between the *RV Martin Bergmann* SST at 1 m and SST at the interface. The most likely explanation is

that even though the *RV Martin Bergmann* measurements are being made close to the surface (at a depth of 1 m), surface

320   stratification in the surface meter is driving the differences being observed. The impact of surface stratification on $pCO_{2\ (sw)}$

has been observed elsewhere in the Arctic (Ahmed et al., 2020;Dong et al., 2021) including for cases where differences can

be up to 200 µatm (Miller et al., 2018). Surface stratification in the Kitikmeot Sea is caused by melting of first-year sea ice

and the large freshwater input by rivers which alone contribute 70 cm of freshwater to the surface annually (Williams et al.,

2018). The fact that the EC tower $pCO_{2\ (sw)}$ was higher than the *RV Martin Bergmann* $pCO_{2\ (sw)}$ would suggest that this is

325   due to river induced stratification as river Arctic riverine water is often higher in $pCO_{2\ (sw)}$ (Cai et al., 2010). Interestingly,

the predicted $pCO_{2\,(sw)}$ from the EC tower show a peak in early August 2017 and a downwards trend through to the end of August, something that is also seen in the ship based $pCO_{2\,(sw)}$ observations (Figure 5b). Similarly, the predicted $pCO_{2\,(sw)}$ from the EC tower increases in August 2018 at a similar rate to the increase seen in the shipboard $pCO_{2\,(sw)}$ observations (Figure 5c). The fact that similar trends can be observed in the *RV Martin Bergmann* and the EC tower $pCO_{2\,(sw)}$ does

330   suggest that seasonal trends in the region are detectable with both methods. The disagreement between the *RV Martin Bergmann* measurements and those from the EC tower highlights the need for year-round $pCO_{2\,(sw)}$ in the flux footprint of the EC tower. Additionally, interfacial $pCO_{2\,(sw)}$ measurements and vertical profiles may help reconcile the observed disparities seen between the two measurement sources of data.

335   There is good agreement in the $pCO_{2\,(sw)}$ values between the EC tower and the ONC mooring in May, June, and October 2017 (Figure 5b) and in May and June 2018 (Figure 5c). The breakdown of stratification at the end of the ice-free summer period and over the winter (Xu et al., 2021) may explain the good agreement between the EC tower and the ONC mooring at these times. In June 2017 the two systems diverge, the $pCO_{2\,(sw)}$ at the ONC mooring decreases due to a spring bloom (Duke et al., 2021) whereas $pCO_{2\,(sw)}$ from the EC tower does not. As the bloom in Cambridge Bay is caused by wastewater

340   discharge (Back et al., 2021) it might be expected that this signal would not detectable at the EC tower.

There appears to be an agreement between the *RV Martin Bergmann* collected data and ONC mooring in the summer of 2016, Unfortunately, the servicing period of the ONC mooring overlapped with the *RV Martin Bergmann* cruise dates meaning there was no period of direct data overlap. The four periods when the *RV Martin Bergmann* was moored up within

345   0.5 km of the mooring on 05:20–11:10 5th August 2016, 05:40–01:20 7/8th August 2016, 08:20–14:30 9th August 2016, 00:50–21:40 10th August 2016 the average $pCO_{2\,(sw)}$ values were 392.58, 384.33, 365.85 and 370.02 µatm respectively. The ONC mooring on 10:00 3rd August was 326.11 and on 12:40 12th August was 371.03. Disagreement between the ONC mooring and the *RV Martin Bergmann* here may be due to different intake depths of the two systems. Stratification may mean the ONC mooring is not representative of $pCO_{2\,(sw)}$ closer to the air-sea interface for parts of ice free period of the year.

350   The spring 2016 measurements from the ONC mooring show that $pCO_{2\,(sw)}$ was high in the spring leading into that field season, the trend towards increasing $pCO_{2\,(sw)}$ due to warming is captured in August 2016 by the ONC mooring and the *RV Martin Bergmann* observations.

Combining the data sources in this way highlights the value of having these different observatories to look at multiyear

355   changes. The observatories provide context to the variability in the summertime $pCO_{2\,(sw)}$ measurements from ships. The patchiness of the measurements from the ONC mooring and the Qikirtaarjuk Island observatory reflects the challenges in making these novel measurements in an extreme environment. Knowledge about how to run them and prevent instrument outages means that future measurements will build towards much needed continuous and complementary multiyear datasets.

4.2 Regional scales – spatial variability in the underway data

360 Focusing back on the *RV Martin Bergmann* data*,* there is clear evidence of spatial regional variability in the underway data. $pCO_{2\ (sw)}$ was typically lower by ~20-40 μatm in the small bays (Cambridge Bay, and Wellington Bay) and larger inlets surveyed (Bathurst Inlet, Chantry Inlet) compared to the central channel (e.g. Dease Strait West, the Finlayson Islands, and Queen Maud Gulf) (Table 1). The reason for relatively lower $pCO_{2\ (sw)}$ in the Bays and Inlets is not readily apparent. For this trend to be driven by temperature, the bays and inlets would need to be ~2°C colder, which was not observed. In fact, many

365 of these regions such as Bathurst Inlet were warmer which would usually predict higher $pCO_{2\ (sw)}$. Although the fluorescence sensor was not robustly calibrated against *in situ* measurements the fluorescence signal was consistent with previous measurements that showed the region to have widespread low primary production at the surface (Martin et al., 2013). Even though these regions did not have consistently higher surface chlorophyll-a concentrations, biological production at depth can not be ruled out as an explanation for lower $pCO_{2\ (sw)}$ in the bays. For example, wastewater discharge

370 has been shown to cause a deep chlorophyll bloom in Cambridge Bay (Back et al., 2021). A large under ice (Arrigo et al., 2012;Mundy et al., 2009) or ice edge (Perrette et al., 2011) phytoplankton bloom could also explain lower values in these bays and inlets. It is possible that these regional differences are driven by regional freshwater inputs; all four identified regions are fed by rivers and there are sharp salinity transitions of ~5 that point to the existence of mixing and fronts (Figure 4c). Rivers are typically thought to be highly oversaturated in $pCO_{2\ (sw)}$ in the Arctic due to organic matter breakdown

375 (Teodoru et al., 2009) so it might be expected that there would be higher $pCO_{2\ (sw)}$ in these bays and inlets. However, whilst the freshwater rivers are high in $pCO_{2\ (sw)}$ (Manning et al., 2020), they are unbuffered and thus have much lower DIC relative to seawater. Dilution by low $pCO_{2\ (sw)}$ ice meltwater does lower $pCO_{2\ (sw)}$ (Cai et al., 2010), a greater impact of ice meltwater in these bays and inlets may be contributing to the lower observed $pCO_{2\ (sw)}$.

380 The ONC mooring is located in Cambridge Bay in shallow water (9 m), at this depth the mooring is not impacted by the Freshwater Creek plume (Duke et al., 2021). It is still unclear how much of an impact being located in the isolated Bay has on the representativeness of these measurements for the Kitikmeot region. As the *RV Martin Bergmann* travelled into and out of the Bay multiple times during the four years of observations, differences in $pCO_{2\ (sw)}$ measured in the Bay and outside the Bay may help identify whether the ONC mooring site is representative of the region as a whole. All transects into and out

385 of Cambridge Bay are shown in Figure 6. Two sub-regions are designated, inside the Bay and outside the Bay, $pCO_{2\ (sw)}$ from the *RV Martin Bergmann* was averaged every two days for which there was data (Table 2). $pCO_{2\ (sw)}$ was largely similar inside and outside of the bay with $pCO_{2\ (sw)}$ typically <±12 μatm. On the 17th August 2017 $pCO_{2\ (sw)}$ was much higher (33.29 μatm) in the Bay, as measurements are similar before (8th/9th) and after (19th/20th) this would point to this being due to something only happening in the Bay; possibly the river plume. Overall, the agreement between the measurements inside

390 and outside of the Bay is encouraging and suggests that $pCO_{2\ (sw)}$ in Cambridge Bay, at least broadly agrees with that in the

main Channel. Without more information, it is difficult to conclude whether the mooring is truly representative of the wider Kitikmeot Sea.
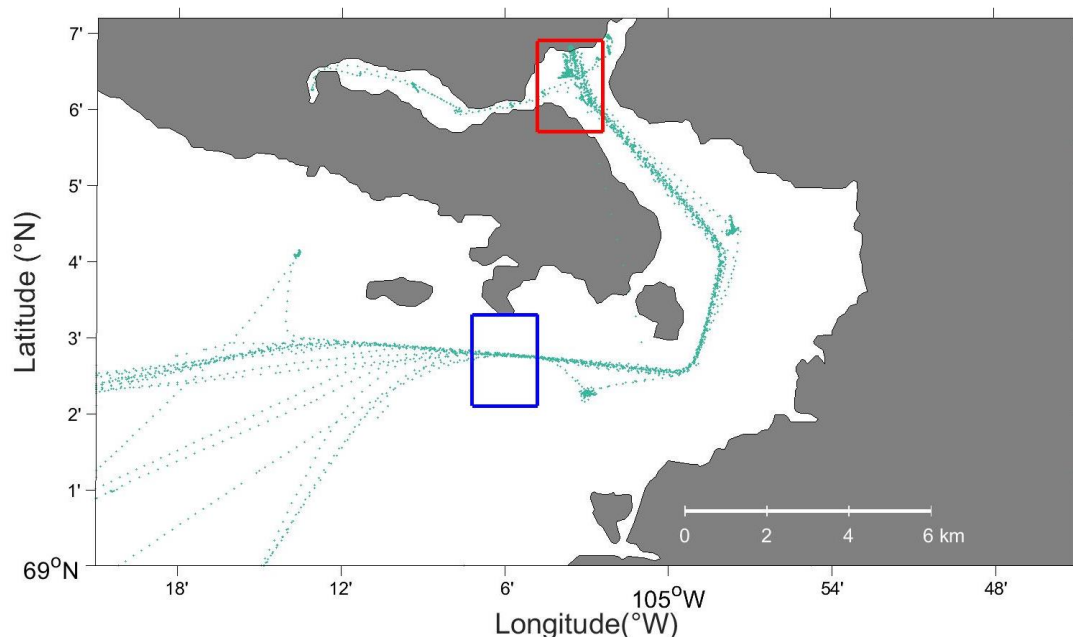
Figure 6: Zoomed in view showing the location of all the $pCO_{2\ (sw)}$ transects (green) measured in and out of Cambridge Bay during the four years of transects. The regions used to define inside the Bay and outside the Bay are shown by a red and blue box respectively.

Table 2: Average $pCO_{2\ (sw)}$ measured by the *RV Martin Bergmann* inside and outside of Cambridge Bay.

Date	$pCO_{2\ (sw)}$ inside Cambridge Bay	$pCO_{2\ (sw)}$ outside Cambridge Bay	$pCO_{2\ (sw)}$ difference (inside Bay –outside Bay)
5th August 2016	405.8	408.0	-2.2
7th - 8th August 2016	424.2	415.5	8.7
9th - 10th August 2016	423.1	412.3	10.8
4th - 5th August 2017	339.1	335.5	3.6
6th - 7th August 2017	340.0	335.4	4.6
8th - 9th August 2017	324.7	325.0	-0.3
17th August 2017	381.5	348.2	33.3
19th - 20th August 2017	334.2	337.5	-3.3

29th August 2017	339.4	339.7	-0.3
31st July - 1st August 2018	196.5	206.2	-9.7
2nd - 3rd August 2018	229.5	220.8	8.7
8th August 2018	194.6	196.0	-1.4
9th August 2019	280.8	292.5	-11.7
18th – 19th August 2019	321.4	327.3	-5.9
21st August 2019	307.7	311.8	-4.1

4.3 Interannual variability and large scale seasonal trends

We have identified local scale differences between the $pCO_{2\,(sw)}$ values from the *RV Martin Bergmann* and the ONC and the Qikirtaarjuk Island observatories and regional scales differences between the bays and inlets and the main channel. The largest differences in the *RV Martin Bergmann* $pCO_{2\,(sw)}$ values occurs between years. The measurement start date of all four cruises spanned a very short window of 10 days (2nd August 2016, 2nd August 2017, 31st July 2018, 9th August 2019). Ahmed et al. (2019) have established the importance of the timing of sea ice breakup on $pCO_{2\,(sw)}$ values in the CAA. During our study, ice breakup began (4th July 2016, 22nd June 2017, 15th July 2018, 14th July 2019) ~2–6 weeks before the start of these cruises. We will now discuss the main controls of the inter–annual variability in the *RV Martin Bergmann* $pCO_{2\,(sw)}$ data.

The very low $pCO_{2\,(sw)}$ values (261 µatm) observed in 2018 (Table 1) could be caused by a combination of low $SST_{(1m)}$, springtime CO_2 depletion by primary production and recent dilution by sea ice melt (Else et al., 2012;Ahmed et al., 2021;Geilfus et al., 2015) or river runoff at salinities >20 (Cai et al., 2010). Without identifying clear chemical signatures that can be attributed to each process it is difficult to say with certainty which of these processes was most important in producing these low $pCO_{2\,(sw)}$ values. As the ice breakup was late in 2018 (resulting in samples collected shortly after breakup), it can be assumed that surface ocean CO_2 exchange with the atmosphere was limited by the ice cover until just before these measurements were made as sea ice is essentially impermeable to gases (Loose et al., 2011;Butterworth and Else, 2018). Additionally, sea ice cover prevented warming of surface seawater as $SST_{(1m)}$ was low in 2018. Light penetrating through sea ice between March and June could have driven primary production below and within the ice (Else et al., 2019). Indeed, an increase in under-ice chlorophyll *a* concentration together with a draw-down of surface nutrients between April to June 2018 supported under-ice phytoplankton production during this period (Dalman et al., 2019). However, concentrations did not exceed 0.6 µg L^{-1}, limited by surface nutrient availability in the region (Back et al., 2021) . It is likely that the melting sea ice stratified the surface and diluted surface $pCO_{2\,(sw)}$ as has been observed in other parts of the Arctic (Miller et al., 2018;Ahmed et al., 2020); low salinity values in the first weeks of the survey support this.

Measurements several weeks into the 2018 cruise show that $pCO_{2(sw)}$ increased quickly in the following weeks likely due to

420   a combination of air–sea exchange and the observed surface warming. Interestingly, at no point during the five years of passing through the Kitikmeot Sea did Ahmed et al. (2019) observe $pCO_{2(sw)}$ values below 300 µatm. Therefore, 2018 could be an anomalously low year for $pCO_{2(sw)}$, or the discrepancy could highlight the fact that (Ahmed et al., 2019) did not make any measurements immediately after breakup in the region. Furthermore, the discrepancy could be influenced by the difference in sampling depth of the two pCO_2 systems between the *CCGS Amundsen* (7 m) and *RV Martin Bergmann* (1 m).

425   The best way to assess the impact of the sampling depth would be to take simultaneous measurements via the ships intake and at the interface as in Ho and Schanze (2020).

Whilst not as heavily undersaturated as 2018, $pCO_{2(sw)}$ was still highly undersaturated with respect to atmospheric values in both 2017 and 2019. In these two years, measurements were made ~4–8 weeks after sea ice breakup and $pCO_{2(sw)}$ values

430   were in the ~300–350 µatm range. Having been ice free for longer, $SST_{(1m)}$ was 3–4 °C warmer in 2017 and 2019 which accounts for much of the $pCO_{2(sw)}$ difference relative to 2018. Warming $SST_{(1m)}$ in 2017 and 2019 and a gradual increase in surface salinity in 2019 mirror the seasonal trends seen in Ahmed et al. (2019) where the CAA becomes saltier and warmer. The 2017 and 2019 $pCO_{2(sw)}$ values are lower than the majority of $pCO_{2(sw)}$ values observed in Coronation Gulf by Ahmed et al. (2019) which again likely reflects the earlier sampling period of this study, where recently ice-free surface waters have

435   not had long to equilibrate with the atmosphere.

$pCO_{2(sw)}$ was much higher in 2016 compared to 2017 and 2019 around four weeks after sea ice breakup. Ahmed et al. (2019) also observed pCO_2 oversaturation in the region in 2016 when they made their observations ~2 weeks later than what we show here. $pCO_{2(sw)}$ oversaturation requires either the upwelling of high $pCO_{2(sw)}$ deep waters, net heterotrophy, or for pCO_2

440    $_{(sw)}$ to be close to equilibrium with the atmosphere and then for the seawater to subsequently heat up (Chierici et al., 2011). The most plausible and observable of these is the warming of the surface waters. It is not apparent why there would be oversaturation in 2016 but not in 2017 and 2019 which were both warmer years if $SST_{(1m)}$ variability was the main factor controlling $pCO_{2(sw)}$. The sea ice breakup time in 2016 was similar to both 2017 and 2019 suggesting that the timing of breakup was also not the only determining factor. The high $pCO_{2(sw)}$ values in 2016 observed under similar conditions to

445   both 2017 and 2019 may point to the importance of the $pCO_{2(sw)}$ value in the previous autumn and wintertime modulation of $pCO_{2(sw)}$. To determine what processes are altering $pCO_{2(sw)}$ between summertime field seasons would require year round sampling or a full biogeochemical model would need to be run over multiple years.

Clearly many interacting processes are involved in determining the $pCO_{2(sw)}$ values in the Kitikmeot Sea. This would

450   indicate that predicting the $pCO_{2(sw)}$ value is difficult. Ahmed et al. (2019) proposed a model for $pCO2_{(sw)}$ in the CAA as a function of weeks since ice breakup, their model underestimated $pCO_{2(sw)}$ in the Kitikmeot Sea by ~26 µatm which they suggest may be due to the impact of rivers. Following their approach, the surface $pCO_{2(sw)}$, SST, and salinity measurements

from this study are presented as a function of time since ice melt (when sea ice concentration declines below 85%; Figure 7). The *RV Martin Bergmann* observations are fairly consistent with the general $p\mathrm{CO}_2$ model of Ahmed et al. (2019), where low

455 $p\mathrm{CO}_{2\,(sw)}$ values (~300 µatm) are seen shortly after sea melt and higher values (~300-350 µatm) are seen in the following two months. However, the 2016 $p\mathrm{CO}_{2\,(sw)}$ values are much higher and the 2018 values are much lower than predicted by the model. The model is also not able to predict the observed salinity values in 2016 and 2019. The CAA flux estimate (Ahmed and Else, 2019) using the (Ahmed et al., 2019) model remains the best estimate for the region. However, the model is clearly unable to capture the full inter–annual variability in the *RV Martin Bergmann* observations. This could be because as a CAA

460 wide model it is not tuned to the Kitikmeot Sea where freshwater inputs are greater. Fundamentally, understanding the drivers of the large interannual variability in $p\mathrm{CO}_{2\,(sw)}$ seen in the Kitikmeot Sea requires an understanding of the interconnected processes involved and their timing. The interannual variability $SST_{(1m)}$ and salinity are comparable to the modelling results of Xu et al. (2021), by expanding on that modelling work with a complex biogeochemical model that can incorporate all the known processes impacting $p\mathrm{CO}_{2\,(sw)}$, it may be possible to accurately reproduce the $p\mathrm{CO}_{2\,(sw)}$

465 observations in this region.
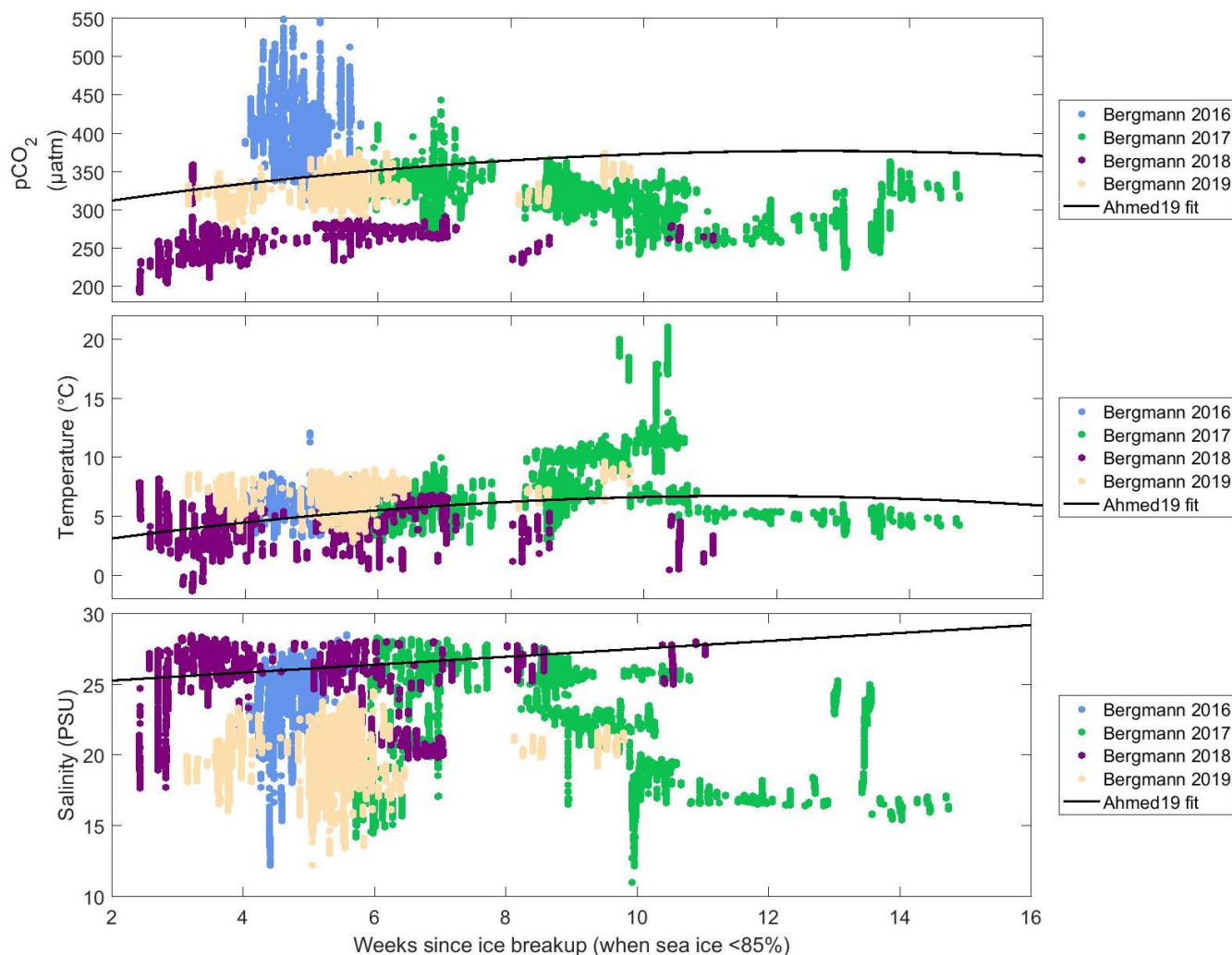
Figure 7: Surface (a) $p\text{CO}_{2\,(sw)}$, (b) SST, and (c) salinity from the *RV Martin Bergmann* as a function of weeks of open water for years 2016 to 2019. Black curves represent the model output of Ahmed and Else (2019).

4.4 The Kitikmeot Sea as a sink for $p\text{CO}2$

The *RV Martin Bergmann* $p\text{CO}_{2\,(sw)}$ measurements indicate that the region is a sink in early August most years (Table 1). At ice breakup low SST $_{(1m)}$ impacts solubility resulting in large $\Delta p\text{CO}_2$ gradients, these conditions persist for several weeks 470 after ice breakup. Warming of the surface when $p\text{CO}_{2\,(sw)}$ is slightly undersaturated is the likely cause of $p\text{CO}_{2\,(sw)}$ oversaturation in some years, resulting in the region becoming a net source once the saturation threshold is met. Whilst not demonstrable with the *RV Martin Bergmann* measurements cooling SST $_{(1m)}$ at the end of the ice-free season should lower $p\text{CO}_{2\,(sw)}$ thereby providing a second period when there are large $\Delta p\text{CO}_2$ gradients. The magnitude of the $\Delta p\text{CO}_2$ and thus the size of the sink throughout the summer appears to not only be driven by time since ice breakup but also by the absolute $p\text{CO}_2$

475   (sw) value at the time of ice breakup. Ahmed and Else (2019) used remote sensing products to identify this region as a net sink when the flux is integrated over the full ice-free period. Our measurements corroborate these findings.

The large variability in $pCO_{2\,(sw)}$ measured in the four years of observations highlights the fact that, in the Arctic, single cruises in only part of the ice-free season are likely not capturing the full variability in these regions. Many $pCO_{2\,(sw)}$ observations in the Arctic are temporally biased towards the middle of the ice-free season. As these single cruises are the

480   only measurements in many of these regions in databases like SOCAT (Bakker et al., 2016), they could result in a biased flux estimates in these regions. It should be acknowledged that the majority of the CAA is not included in the state of the art observational based products (Landschützer et al., 2020).

5. Conclusions

The ONC mooring and EC tower both provide similar $pCO_{2\,(sw)}$ values in spring and autumn showing good agreement

485   between the two platforms. Measured $pCO_{2\,(sw)}$ from the EC tower was much higher than what was measured from the *RV Martin Bergmann* but similar trends were seen in both data sources which may be attributable to surface stratification caused by riverine flows. Comparing measurements collected by the *RV Martin Bergmann* in and out of Cambridge Bay indicates that Cambridge Bay $pCO_{2\,(sw)}$ is not drastically different from the main channel in August. This may indicate that $pCO_{2\,(sw)}$ at the ONC mooring may be broadly representative of Dease Strait.

490

The Kitikmeot Sea was a CO_2 sink or a very week source over the summers of 2016 – 2019, consistent with previous measurements from Ahmed and Else (2019). The CO_2 sink was highly variable from year to year at the beginning of August (average observed fluxes of 0.41, -7.70, -21.26 and -2.08 mmol m^{-2} d^{-1} during the 2016, 2017, 2018, and 2019 cruises respectively) with average $pCO_{2\,(sw)}$ as low as 261.19 ± 19.70 µatm and as high as 403.65 ± 44.44 µatm. $pCO_{2\,(sw)}$ was much

495   lower in 2018 due to the much lower SST $_{(1m)}$ that year. The magnitude of the ΔpCO_2 throughout the summer appears to be controlled by the absolute $pCO_{2\,(sw)}$ value at the time of ice breakup. Low $pCO_{2\,(sw)}$ values increase in August due to exchange with the atmosphere and warming broadly following the predicted trends using the model developed by Ahmed et al. (2019). In years where $pCO_{2\,(sw)}$ is high when ice breakup occurs, warming can cause a period of slight $pCO_{2\,(sw)}$ oversaturation in summer, in these situations the magnitude of this oversaturation is likely moderated by the air sea flux

500   reducing $pCO_{2\,(sw)}$. $pCO_{2\,(sw)}$ was found to be ~20-40 µatm lower in the Bays and Inlets that were surveyed; this could be driven by freshwater inputs into these isolated regions. Lower pCO_2 in bays and inlets would represent an observational bias in the CAA-wide surveys (Ahmed et al., 2019). Freshwater fluxes into the southern CAA are much greater than elsewhere in the CAA meaning that this bias might be more prominent in the Kitikmeot Sea. Further observations in these regions may complement the basin-level pCO_2 mapping.

505

These findings provide a more nuanced picture of the considerable inter-annual variability in $pCO_{2\ (sw)}$ observed during repeat cruises in the same region, underscoring how much may be missed by relying on data collected during one-off cruises along the dynamic Arctic coasts. The $pCO_{2\ (sw)}$ at the time of ice melt is very important as it dictates the magnitude and direction of the flux for much of the ice-free period. A better understanding of $pCO_{2\ (sw)}$ through the ice covered period is needed to help unravel the seasonal and interannual variability.

6. Acknowledgements

Parts of this research were completed on or adjacent to Inuit Owned Lands under the authority of the Nunavut Land Claim Agreement, and the work was licensed by the Nunavut Research Institute. We thank the Ekaluktutiak Hunters and Trappers Organization and the community of Cambridge Bay for their hospitality and support of this project. Richard Sims was supported through the University of Calgary's Eyes High Postdoctoral fellowship program. This work was funded by The Marine Environmental Observation, Prediction and Response Network (MEOPAR, project number 1-02-02-004.1), The Kitikmeot Sea Science Study (K3S), the Natural Sciences and Engineering Research Council of Canada (Discovery and Northern Research Supplement grants to B. Else, RGPIN-2015-04780), and the Canada Foundation for Innovation (John R. Edwards Leaders Fund grant to B. Else, 34814). Logistical support was provided by the Arctic Research Foundation. Samantha Jones, Stephen Gonski and Patrick Duke were supported by Polar Knowledge Canada through the Northern Scientific Training Program. We thank Polar Knowledge Canada and the Canadian High Arctic Research Station for their support and for providing accommodation and vehicles during field campaigns. Data from Ocean Networks Canada was accessed under their Creative Commons CC-BY 4.0 License. We thank the captain and crew of the *RV Martin Bergmann* for all their assistance. We also thank Shawn Marriott and Francis Emingak for all their assistance in the field, and Sophia Ahmed for her work on data interpretation.

7. Author Contributions

This manuscript was written by RPS, all co-authors made contributions to the final paper. BTGE installed the underway system at the start of each field season. The performance of the underway system was monitored by BTGE with help from SFJ, SFG, KAB, PJD and RPS. RPS organised and processed the data. RPS made the figures and interpreted the results and with support from MA and BTGE. BJB analysed the data from the EC tower and provided that data for this paper. PJD provided the data from the ONC mooring. BTGE, CJM and WJW secured have been central in planning the cruise programme. BTGE oversaw completion of the work.

8. Data and code availability

The processed underway data from the *RV Martin Bergmann* which is the new data described in this paper is available in the

535 supplement as .mat files. The raw and processed underway data from the *RV Martin Bergmann* data will also be available via Zenodo. The wind data and inferred seawater pCO_2 data from the EC tower are included in the supplement as .mat files. The ONC mooring data is freely available at https://data.oceannetworks.ca/home. The AMSR2 sea ice data https://seaice.uni-bremen.de/data/amsr2/asi_daygrid_swath/n3125/ the NCEP winds https://psl.noaa.gov/data/gridded/data.ncep.reanalysis2.html and the atmospheric pCO_2 data from Barrow

540 ftp://aftp.cmdl.noaa.gov/data/greenhouse_gases/co2/in-situ/surface/ which were used in this paper are all freely available from their online repositories. Processing code and the code needed to reproduce the figures was written in Matlab 2016a. The code is provided in the supplement and is also available at https://github.com/Richard-Sims/Sims_2022_Bergmann_pCO2.

References

545 Ahmed, M., Else, B., Burgers, T., and Papakyriakou, T.: Variability of surface water pCO2 in the Canadian Arctic Archipelago from 2010 to 2016, Journal of Geophysical Research: Oceans, 124, 1876-1896, https://doi.org/10.1029/2018JC014639, 2019.

Ahmed, M., and Else, B. G.: The Ocean CO2 Sink in the Canadian Arctic Archipelago: A Present-Day Budget and Past Trends Due to Climate Change, Geophysical research letters, 46, 9777-9785, https://doi.org/10.1029/2019GL083547, 2019.

550 Ahmed, M. M., Else, B. G., Capelle, D., Miller, L. A., and Papakyriakou, T.: Underestimation of surface pCO2 and air-sea CO2 fluxes due to freshwater stratification in an Arctic shelf sea, Hudson Bay, Elementa: Science of the Anthropocene, 8, 084, https://doi.org/10.1525/elementa.084, 2020.

Ahmed, M. M., Else, B. G., Butterworth, B., Capelle, D. W., Guéguen, C., Miller, L. A., Meilleur, C., and Papakyriakou, T.: Widespread surface water p CO2 undersaturation during ice-melt season in an Arctic continental shelf sea (Hudson Bay,

555 Canada), Elem Sci Anth, 9, 00130, https://doi.org/10.1525/elementa.2020.00130, 2021.

Arrigo, K. R., Perovich, D. K., Pickart, R. S., Brown, Z. W., Van Dijken, G. L., Lowry, K. E., Mills, M. M., Palmer, M. A., Balch, W. M., and Bahr, F.: Massive phytoplankton blooms under Arctic sea ice, Science, 336, 1408-1408, DOI: 10.1126/science.1215065, 2012.

Back, D.-Y., Ha, S.-Y., Else, B., Hanson, M., Jones, S. F., Shin, K.-H., Tatarek, A., Wiktor, J. M., Cicek, N., and Alam, S.:

560 On the impact of wastewater effluent on phytoplankton in the Arctic coastal zone: a case study in the Kitikmeot Sea of the Canadian Arctic, Science of The Total Environment, 764, 143861, https://doi.org/10.1016/j.scitotenv.2020.143861, 2021.

Bakker, D. C., Pfeil, B., Landa, C. S., Metzl, N., O'brien, K. M., Olsen, A., Smith, K., Cosca, C., Harasawa, S., and Jones, S. D.: A multi-decade record of high-quality fCO 2 data in version 3 of the Surface Ocean CO 2 Atlas (SOCAT), Earth System Science Data, 8, 383, https://doi.org/10.5194/essd-8-383-2016, 2016.

565 Bates, N., and Mathis, J.: The Arctic Ocean marine carbon cycle: evaluation of air-sea CO 2 exchanges, ocean acidification impacts and potential feedbacks, Biogeosciences, 6, 2433-2459, doi:10.5194/bg-6-2433-2009, 2009.

Butterworth, B. J., and Else, B. G.: Dried, closed-path eddy covariance method for measuring carbon dioxide flux over sea ice, Atmospheric Measurement Techniques, 11, 6075-6090, https://doi.org/10.5194/amt-11-6075-2018, 2018.

Butterworth, B. J., Else, B. G., Brown, K. A., Mundy, C. J., Rotermund, L. M., William, W. J., and Boer, G. d.: Annual

570 carbon dioxide flux over seasonal sea ice in the Canadian Arctic, In prep, 2022.

Cai, W.-J., Chen, L., Chen, B., Gao, Z., Lee, S. H., Chen, J., Pierrot, D., Sullivan, K., Wang, Y., and Hu, X.: Decrease in the CO2 uptake capacity in an ice-free Arctic Ocean basin, Science, 329, 556-559, DOI: 10.1126/science.1189338, 2010.

Chierici, M., Fransson, A., Lansard, B., Miller, L. A., Mucci, A., Shadwick, E., Thomas, H., Tremblay, J., and Papakyriakou, T. N.: Impact of biogeochemical processes and environmental factors on the calcium carbonate saturation state in the Circumpolar Flaw Lead in the Amundsen Gulf, Arctic Ocean, Journal of Geophysical Research: Oceans, 116, https://doi.org/10.1029/2011JC007184, 2011.

Cruz-García, R., Ortega, P., Guemas, V., Acosta Navarro, J. C., Massonnet, F., and Doblas-Reyes, F. J.: An anatomy of Arctic sea ice forecast biases in the seasonal prediction system with EC-Earth, Climate Dynamics, 56, 1799-1813, https://doi.org/10.1007/s00382-020-05560-4, 2021.

Dalman, L. A., Else, B. G., Barber, D., Carmack, E., Williams, W. J., Campbell, K., Duke, P. J., Kirillov, S., Mundy, C. J., and Tremblay, J.-É.: Enhanced bottom-ice algal biomass across a tidal strait in the Kitikmeot Sea of the Canadian Arctic, Elementa: Science of the Anthropocene, 7, https://doi.org/10.1525/elementa.361, 2019.

DeGrandpre, M., Evans, W., Timmermans, M. L., Krishfield, R., Williams, B., and Steele, M.: Changes in the Arctic Ocean carbon cycle with diminishing ice cover, Geophysical research letters, 47, e2020GL088051, https://doi.org/10.1002/essoar.10502603.1, 2020.

Dickson, A. G., Sabine, C. L., and Christian, J. R.: Guide to best practices for ocean CO_2 measurements, North Pacific Marine Science Organization, Sidney, British Columbia, 191, 2007.

Dong, Y., Yang, M., Bakker, D. C., Liss, P. S., Kitidis, V., Brown, I., Chierici, M., Fransson, A., and Bell, T. G.: Near-Surface Stratification Due to Ice Melt Biases Arctic Air-Sea CO2 Flux Estimates, Geophysical research letters, 48, e2021GL095266, https://doi.org/10.1029/2021GL095266, 2021.

Duke, P., Else, B., Jones, S., Marriot, S., Ahmed, M., Nandan, V., Butterworth, B., Gonski, S., Dewey, R., and Sastri, A.: Seasonal marine carbon system processes in an Arctic coastal landfast sea ice environment observed with an innovative underwater sensor platform, Elementa: Science of the Anthropocene, 9, 00103, https://doi.org/10.1525/elementa.2021.00103, 2021.

Else, B., Galley, R., Papakyriakou, T., Miller, L., Mucci, A., and Barber, D.: Sea surface pCO2 cycles and CO2 fluxes at landfast sea ice edges in Amundsen Gulf, Canada, Journal of Geophysical Research: Oceans, 117, https://doi.org/10.1029/2012JC007901, 2012.

Else, B. G., Whitehead, J. J., Galindo, V., Ferland, J., Mundy, C., Gonski, S. F., Ehn, J. K., Rysgaard, S., and Babin, M.: Response of the Arctic marine inorganic carbon system to ice algae and under-ice phytoplankton blooms: A case study along the fast-ice edge of Baffin Bay, Journal of Geophysical Research: Oceans, 124, 1277-1293, https://doi.org/10.1029/2018JC013899, 2019.

Evans, W., Pocock, K., Hare, A., Weekes, C., Hales, B., Jackson, J., Gurney-Smith, H., Mathis, J. T., Alin, S. R., and Feely, R. A.: Marine CO2 patterns in the northern salish sea, Frontiers in Marine Science, 5, 536, https://doi.org/10.3389/fmars.2018.00536, 2019.

Ford, J. D., Smit, B., Wandel, J., Allurut, M., Shappa, K., Ittusarjuat, H., and Qrunnut, K.: Climate change in the Arctic: current and future vulnerability in two Inuit communities in Canada, Geographical Journal, 174, 45-62, https://doi.org/10.1111/j.1475-4959.2007.00249.x, 2008.

Geilfus, N.-X., Galley, R., Crabeck, O., Papakyriakou, T., Landy, J., Tison, J.-L., and Rysgaard, S.: Inorganic carbon dynamics of melt-pond-covered first-year sea ice in the Canadian Arctic, Biogeosciences, 12, 2047-2061, https://doi.org/10.5194/bg-12-2047-2015, 2015.

Geilfus, N.-X., Pind, M., Else, B., Galley, R., Miller, L., Thomas, H., Gosselin, M., Rysgaard, S., Wang, F., and Papakyriakou, T.: Spatial and temporal variability of seawater pCO2 within the Canadian Arctic Archipelago and Baffin Bay during the summer and autumn 2011, Continental Shelf Research, 156, 1-10, 2018.

Harris, L. N., Yurkowski, D. J., Gilbert, M. J., Else, B. G., Duke, P. J., Ahmed, M. M., Tallman, R. F., Fisk, A. T., and Moore, J.: Depth and temperature preference of anadromous Arctic char Salvelinus alpinus in the Kitikmeot Sea, a shallow and low-salinity area of the Canadian Arctic, Marine Ecology Progress Series, 634, 175-197, https://doi.org/10.3354/meps13195, 2020.

Ho, D. T., and Schanze, J. J.: Precipitation-Induced Reduction in Surface Ocean pCO2: Observations From the Eastern Tropical Pacific Ocean, Geophysical research letters, 47, e2020GL088252, https://doi.org/10.1029/2020GL088252, 2020.

JCGM: Evaluation of measurement data—Guide to the expression of uncertainty in measurement, 134, 2008.

Kalnay, E., Kanamitsu, M., Kistler, R., Collins, W., Deaven, D., Gandin, L., Iredell, M., Saha, S., White, G., and Woollen, J.: The NCEP/NCAR 40-year reanalysis project, Bulletin of the American Meteorological Society, 77, 437-472, https://doi.org/10.1175/1520-0477(1996)077<0437:TNYRP>2.0.CO;2, 1996.

Kim, K., Ha, S.-Y., Kim, B. K., Mundy, C., Gough, K. M., Pogorzelec, N. M., and Lee, S. H.: Carbon and nitrogen uptake rates and macromolecular compositions of bottom-ice algae and phytoplankton at Cambridge Bay in Dease Strait, Canada, Annals of Glaciology, 61, 106-116, https://doi.org/10.1017/aog.2020.17, 2020.

Landrum, L., and Holland, M. M.: Extremes become routine in an emerging new Arctic, Nature Climate Change, 10, 1108-1115, https://doi.org/10.1038/s41558-020-0892-z
2020.

Landschützer, P., Laruelle, G. G., Roobaert, A., and Regnier, P.: A uniform pCO2 climatology combining open and coastal oceans, Earth System Science Data, 12, 2537-2553, https://doi.org/10.5194/essd-12-2537-2020, 2020.

Loose, B., Schlosser, P., Perovich, D., Ringelberg, D., Ho, D., Takahashi, T., Richter-Menge, J., Reynolds, C., McGillis, W., and Tison, J.-L.: Gas diffusion through columnar laboratory sea ice: implications for mixed-layer ventilation of CO2 in the seasonal ice zone, Tellus B: Chemical and Physical Meteorology, 63, 23-39, https://doi.org/10.1111/j.1600-0889.2010.00506.x, 2011.

Macdonald, R., Anderson, L., Christensen, J., Miller, L., Semiletov, I., and Stein, R.: The Arctic Ocean: budgets and fluxes, in: Carbon and Nutrient Fluxes in Continental Margins: A Global Synthesis, , edited by: Liu, K., Atkinson, , L., Q., and R., T.-M., Springer-Verlag, Berlin Heidelberg, 291–303, 2010.

Manning, C. C., Preston, V. L., Jones, S. F., Michel, A. P., Nicholson, D. P., Duke, P. J., Ahmed, M. M., Manganini, K., Else, B. G., and Tortell, P. D.: River inflow dominates methane emissions in an Arctic coastal system, Geophysical research letters, 47, e2020GL087669, https://doi.org/10.1029/2020GL087669, 2020.

Martin, J., Dumont, D., and Tremblay, J. É.: Contribution of subsurface chlorophyll maxima to primary production in the coastal Beaufort Sea (Canadian Arctic): A model assessment, Journal of Geophysical Research: Oceans, 118, 5873-5886, https://doi.org/10.1002/2013JC008843, 2013.

Miller, L. A., Burgers, T. M., Burt, W. J., Granskog, M. A., and Papakyriakou, T. N.: Air-Sea CO2 Flux Estimates in Stratified Arctic Coastal Waters: How Wrong Can We Be?, Geophysical research letters, 46, 235-243, https://doi.org/10.1029/2018GL080099, 2018.

Mundy, C., Gosselin, M., Ehn, J., Gratton, Y., Rossnagel, A., Barber, D. G., Martin, J., Tremblay, J. É., Palmer, M., and Arrigo, K. R.: Contribution of under-ice primary production to an ice-edge upwelling phytoplankton bloom in the Canadian Beaufort Sea, Geophysical research letters, 36, https://doi.org/10.1029/2009GL038837, 2009.

Nightingale, P. D., Malin, G., Law, C. S., Watson, A. J., Liss, P. S., Liddicoat, M. I., Boutin, J., and Upstill-Goddard, R. C.: In situ evaluation of air-sea gas exchange parameterizations using novel conservative and volatile tracers, Global Biogeochemical Cycles, 14, 373-387, https://doi.org/10.1029/1999GB900091, 2000.

Parmentier, F.-J. W., Christensen, T. R., Sørensen, L. L., Rysgaard, S., McGuire, A. D., Miller, P. A., and Walker, D. A.: The impact of lower sea-ice extent on Arctic greenhouse-gas exchange, Nature Climate Change, 3, 195-202, https://doi.org/10.1038/nclimate1784, 2013.

Perrette, M., Yool, A., Quartly, G., and Popova, E. E.: Near-ubiquity of ice-edge blooms in the Arctic, Biogeosciences, 8, 515-524, https://doi.org/10.5194/bg-8-515-2011, 2011.

Peterson, J. T., Komhyr, W., Waterman, L., Gammon, R., Thoning, K., and Conway, T.: Atmospheric CO2 variations at Barrow, Alaska, 1973–1982, in: Scientific Application of Baseline Observations of Atmospheric Composition (SABOAC), edited by: Ehhalt, D., Pearman, G., and Galbally, I., Springer, Dordrecht, 397-416, 1987.

Sims, R. P., Schuster, U., Watson, A. J., Yang, M. X., Hopkins, F. E., Stephens, J., and Bell, T. G.: A measurement system for vertical seawater profiles close to the air–sea interface, Ocean Science, 13, 649-660, https://doi.org/10.5194/os-13-649-2017, 2017.

Spreen, G., Kaleschke, L., and Heygster, G.: Sea ice remote sensing using AMSR-E 89-GHz channels, Journal of Geophysical Research: Oceans, 113, https://doi.org/10.1029/2005JC003384, 2008.

Takahashi, T., Olafsson, J., Goddard, J. G., Chipman, D. W., and Sutherland, S.: Seasonal variation of CO2 and nutrients in the high-latitude surface oceans: A comparative study, Global Biogeochemical Cycles, 7, 843-878, https://doi.org/10.1029/93GB02263, 1993.

670   Teodoru, C. R., Del Giorgio, P. A., Prairie, Y. T., and Camire, M.: Patterns in pCO2 in boreal streams and rivers of northern Quebec, Canada, Global Biogeochemical Cycles, 23, https://doi.org/10.1029/2008GB003404, 2009.

Wang, Q., Myers, P. G., Hu, X., and Bush, A. B.: Flow constraints on pathways through the Canadian Arctic Archipelago, Atmosphere-Ocean, 50, 373-385, https://doi.org/10.1080/07055900.2012.704348, 2012.

Wanninkhof, R.: Relationship between wind speed and gas exchange over the ocean revisited, Limnology and
675   Oceanography: Methods, 12, 351-362, https://doi.org/10.4319/lom.2014.12.351, 2014.

Weiss, R. F.: Carbon dioxide in water and seawater: the solubility of a non-ideal gas, Marine chemistry, 2, 203-215, http://dx.doi.org/10.1016/0304-4203(74)90015-2, 1974.

Wessel, P., and Smith, W. H.: A global, self-consistent, hierarchical, high-resolution shoreline database, Journal of Geophysical Research: Solid Earth, 101, 8741-8743, https://doi.org/10.1029/96JB00104, 1996.

680   Williams, W., Brown, K. A., Bluhm, B., Carmack, E. C., Dalman, L., Danielson, S. L., Else, B. G., Friedriksen, R., Mundy, C., and Rotermund, L. M.: Stratification in the Canadian Arctic Archipelago's Kitikmeot Sea: biological and geochemical consequences, Polar Knowledge Canada, Ottawa, Canada, 46-52, 2018.

Woolf, D. K., Shutler, J. D., Goddijn-Murphy, L., Watson, A., Chapron, B., Nightingale, P. D., Donlon, C. J., Piskozub, J., Yelland, M., and Ashton, I.: Key uncertainties in the recent air-sea flux of CO2, Global Biogeochemical Cycles, 33, 1548-
685   1563, https://doi.org/10.1029/2018GB006041, 2019.

Wynja, V., Demers, A.-M., Laforest, S., Lacelle, M., Pasher, J., Duffe, J., Chaudhary, B., Wang, H., and Giles, T.: Mapping coastal information across Canada's northern regions based on low-altitude helicopter videography in support of environmental emergency preparedness efforts, Journal of Coastal Research, 31, 276-290, https://doi.org/10.2112/JCOASTRES-D-14-00059.1, 2015.

690   Xu, C., Mikhael, W., Myers, P. G., Else, B., Sims, R. P., and Zhou, Q.: Effects of Seasonal Ice Coverage on the Physical Oceanographic Conditions of the Kitikmeot Sea in the Canadian Arctic Archipelago, Atmosphere-Ocean, 59, 1-19, https://doi.org/10.1080/07055900.2021.1965531, 2021.